

# Modeling of cyclic shear-flexure interaction in reinforced concrete structural walls

**K. Kolozvari, T. Tran, & J. Wallace**

*University of California at Los Angeles, Los Angeles, California, USA*

**K. Orakcal**

*Bogazici University, Istanbul, Turkey*



## SUMMARY:

Existing approaches used to model the lateral force versus deformation responses of reinforced concrete (RC) walls typically assume uncoupled axial/flexural and shear responses. An analytical model that captures the interaction between these responses for RC walls subjected to reversed-cyclic loading conditions is described. The proposed modeling approach incorporates RC panel behavior into a two-dimensional fiber-based macroscopic model. The coupling of axial and shear responses is achieved at the fiber (panel) level, which further allows coupling of flexural and shear responses at the element level. The behavior of RC panel elements under generalized, in-plane, reversed-cyclic loading conditions is described with a constitutive RC panel model based on an interpretation of the so-called fixed-strut-angle panel model. The analytical model is verified by comparing the experimentally measured and analytically predicted cyclic responses of two heavily-instrumented RC wall specimens, experiencing significant shear-flexure interaction behavior. Good correlations between experimental and analytical results are achieved.

*Keywords: reinforced concrete, structural walls, analytical modelling, shear-flexure interaction*

## 1. INTRODUCTION

Reinforced concrete (RC) structural walls are one of the most commonly used systems in buildings to resist wind and earthquake loads worldwide. A large percentage of the walls constructed are commonly classified as moderately slender, with wall height-to-length ratio (aspect ratio) between approximately 1.5 and 3.0, where both nonlinear flexural and shear deformations may significantly contribute to the lateral load response. Low aspect ratio walls (less than 1.0) are typically dominated by shear behavior and taller walls (aspect ratio greater than 3.0) are generally dominated by flexural responses. For moderate aspect ratio walls flexural yielding is expected; however, nonlinear shear deformations are typically significant and lead to reduced stiffness and sometimes reduced strength.

According to experimental evidence, the interaction between flexural and shear deformations exists even for relatively slender RC walls with aspect ratios of 3.0 and 4.0, with shear deformations contributing to lateral deformations by approximately 30% and 10% of the first story and roof-level lateral displacement, respectively (Barda et al., 1976; Massone and Wallace, 2004). Experimental results have shown that shear deformations for RC walls with aspect ratios of 1.5 and 2.0 contribute as much as 35% and 30% of the wall top displacement, respectively (Tran and Wallace, 2012). A majority of existing analytical models for predicting nonlinear behavior of RC walls do not incorporate shear-flexure interaction (SFI) and describe the shear behavior of a wall using ad-hoc force deformation rules defined independently from the flexural modeling parameters. Modeling approaches that do capture this interaction are limited to ad-hoc models or empirically-based models (e.g. Xu and Zhang, 2010; Beyer et al., 2011) or models that are limited to monotonic responses only (Massone et al., 2006). In addition, none of the modeling approaches have been validated in any significant way, since the detailed data needed, especially for localized responses for cases with significant interaction, are not available. A formulation of a robust modeling approach for cyclic SFI is presented along with the

preliminary model validation using new test data presented in a companion paper (Tran and Wallace, 2012).

## 2. ANALYTICAL MODEL DESCRIPTION AND BACKGROUND

The proposed analytical model incorporates RC panel behavior into a two-dimensional macroscopic fiber model in order to capture the experimentally observed SFI in RC walls. In this study, the Multiple-Vertical-Line-Element-Model (MVLEM) developed by Orakcal et al. (2004) is chosen as the baseline model for implementation of a new cyclic SFI model. This model is chosen because of its relatively simple formulation, numerical stability, and reasonably accurate predictions of flexural responses (Orakcal and Wallace, 2006). The original formulation of the MVLEM, with uncoupled shear and flexural responses, is modified by replacing each uniaxial (macro-fiber) element with a RC panel element subjected to membrane actions (Fig. 2.1). This enables coupling of axial and shear responses at the panel (fiber) level, which further allows coupling of flexural and shear responses at the model element level. The constitutive RC panel behavior under generalized reversed-cyclic loading conditions is described by the Fixed-Strut-Angle-Model (FSAM) developed by Ulugtekin (2010), which was shown to replicate the results of cyclic panel tests available in the literature with reasonable accuracy. Massone et al. (2006) proposed a conceptually similar modeling approach to capture monotonic responses using a constitutive RC panel behavior described by a rotating-crack angle model (RSAM); however, extensions to capture cyclic responses proved cumbersome.

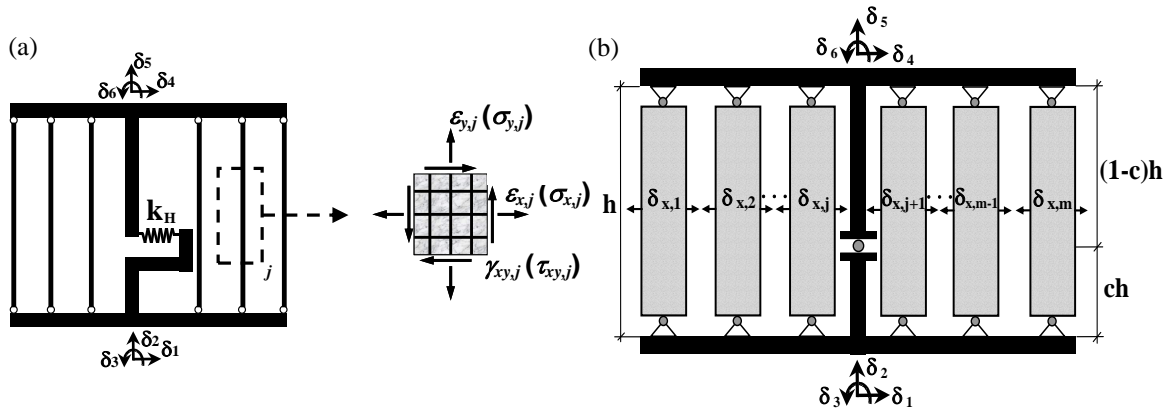


Figure 2.1. Element models: (a) original MVLEM element and (b) coupled SFI model element

### 2.1. Implemented RC panel behavior

The constitutive RC panel model implemented here to model SFI for structural walls is based on several simplifying assumptions: (i) perfect bond between concrete and reinforcement, (ii) zero dowel action on reinforcement, and (iii) directions (angles) of concrete compression struts (along which concrete follows biaxial stress-strain relationships) coincide with the directions of the cracks. Concrete biaxial stress-strain relationships are used to represent behavior of compressions struts, the orientation of which remain unchanged after cracking occurs, while the behavior of reinforcing bars is described by uniaxial stress-strain relationships. The formulation of the constitutive panel model is characterized by the three stages of RC panel behavior: (a) uncracked concrete, (b) behavior after formation of the first crack, and (c) behavior after formation of the second crack.

In the initial model formulation, aggregate interlock effects are ignored and shear stresses along cracks are assumed to be zero. The initial assumption of zero aggregate interlock (zero shear stress along cracks) resulted in a significant overestimation of shear deformations by the SFI model (when compared to experimental results), due to deformation associated with sliding shear along diagonal cracks. Therefore, in the implementation described here, the shear stress versus shear (sliding) strain

behavior along cracks is simulated by a simple linear-elastic (nearly rigid) shear aggregate interlock constitutive model:

$$\tau_{cr} = G_c \cdot \gamma_{cr} \quad (2.1)$$

where  $G_c$  is the elastic concrete shear modulus, which is taken as  $0.4E_c$ , where  $E_c$  is the Young's modulus for concrete. Use of this relation assumes that shear aggregate interlock behavior is not affected by crack characteristics (e.g. widths, opening and closing), which is not realistic; however, a simple relationship was assumed to enable model results to be assessed for the extreme case where sliding along cracks is restrained.

## 2.2. Material constitutive models for concrete and reinforcing steel

Since the implemented constitutive RC panel model relates the panel response directly to uniaxial constitutive stress-strain behavior of concrete and reinforcing steel, state-of-the-art hysteretic material constitutive relationships were implemented.

The implemented uniaxial constitutive stress-strain relationship for reinforcing steel is the well-known nonlinear hysteretic model of Menegotto and Pinto (1973), extended by Filippou et al. (1983) to include isotropic strain hardening effects. The model is simple in its formulation and computationally efficient, yet is capable of reproducing experimental results with reasonable accuracy, via capturing the important behavioral features of the hysteretic behavior of reinforcing steel bars (i.e. Bauschinger's effect, kinematic and isotropic strain hardening, tension stiffening).

The uniaxial hysteretic constitutive model proposed by Chang and Mander (1994) was adopted in this study to represent the uniaxial stress-strain behavior of concrete. The Chang and Mander model is an advanced, rule-based, generalized, and non-dimensional constitutive model that can simulate the hysteretic behavior of confined and unconfined, ordinary and high-strength concrete in both cyclic compression and tension. The model addresses important behavioral issues such as hysteretic behavior in both cyclic compression and tension, progressive stiffness degradation associated with unloading and reloading curves at increasing strain values, and effects of gradual crack closure. Minor modifications to the original formulation of the Chang and Mander model were required to represent behavioral features of concrete under biaxial loading, such as inclusion of parameters to represent compression softening, hysteretic biaxial damage, and tension stiffening. Details of these parameters are provided by Ulugtekin (2010).

## 2.3. Model formulation

In the modified MVLEM formulation to incorporate SFI, the longitudinal normal (axial) strain  $\varepsilon_y$  and shear strain  $\gamma_{xy}$  values are first calculated for the entire wall cross section (for all panel macro-fibers) based on six prescribed degrees of freedom defined at the top and bottom rigid beams of the model element  $\{\delta_N\} = \{\delta_1 \delta_2 \dots \delta_6\}^T$  (Fig. 2.1a). Plane-sections-remain-plane is assumed and shear strain is assumed to be uniformly distributed along the wall section. Horizontal normal strain  $\varepsilon_x$  on each RC panel element (which is necessary to complete the strain field in each panel), is defined by use of additional degrees of freedom in the horizontal direction  $\{\delta_x\} = \{\delta_{x,1} \delta_{x,2} \dots \delta_{x,m}\}^T$  (where  $m$  is the number of panel macro-fibers in one model element) as shown on Fig. 2.1b. These horizontal (extensional) degrees of freedom on the panel macro-fibers are assumed to be kinematically independent from the six nodal displacement degrees of freedom at the top and bottom of the element; therefore, the total degrees of freedom necessary to describe the deformation of one modified MVLE is increased, from 6 in the original formulation of the MVLEM, to  $6+m$ .

For any level of deformation (strain) imposed on each RC panel ( $\varepsilon_x$ ,  $\varepsilon_y$  and  $\gamma_{xy}$ ), the stiffness properties and force-deformation relationships of the panel macro-fibers are defined according to the implemented constitutive panel model and the tributary areas of concrete and reinforcing steel

assigned to each panel macro-fiber. Since the deformation on each RC panel element is described by three strain degrees of freedom ( $\varepsilon_x$ ,  $\varepsilon_y$  and  $\gamma_{xy}$ ), the tangent stiffness properties of a single constitutive panel element are given by the following 3x3 partial stiffness matrix:

$$[K_p]_j = \begin{bmatrix} \frac{\partial \sigma_x}{\partial \varepsilon_x} & \frac{\partial \sigma_x}{\partial \varepsilon_y} & \frac{\partial \sigma_x}{\partial \gamma_{xy}} \\ \frac{\partial \sigma_y}{\partial \varepsilon_x} & \frac{\partial \sigma_y}{\partial \varepsilon_y} & \frac{\partial \sigma_y}{\partial \gamma_{xy}} \\ \frac{\partial \tau_{xy}}{\partial \varepsilon_x} & \frac{\partial \tau_{xy}}{\partial \varepsilon_y} & \frac{\partial \tau_{xy}}{\partial \gamma_{xy}} \end{bmatrix}_j \quad (2.2)$$

Axial stiffness in  $x$  and  $y$  directions  $k_{x,j}$  and  $k_{y,j}$ , and shear stiffness  $k_{H,j}$  of the  $j$ -th RC panel element are then obtained from the panel partial stiffness, considering the geometric properties of each panel element (panel macro-fiber), as:

$$k_{x,j} = \left( \frac{\partial F_x}{\partial u_x} \right)_j = \left( \frac{\partial F_x}{\partial \sigma_x} \right)_j \cdot \left( \frac{\partial \sigma_x}{\partial \varepsilon_x} \right)_j \cdot \left( \frac{\partial \varepsilon_x}{\partial u_x} \right)_j = \left( \frac{\partial \sigma_x}{\partial \varepsilon_x} \right)_j \cdot \frac{h \cdot t}{b_j} \quad (2.3)$$

$$k_{y,j} = \left( \frac{\partial F_y}{\partial u_y} \right)_j = \left( \frac{\partial F_y}{\partial \sigma_y} \right)_j \cdot \left( \frac{\partial \sigma_y}{\partial \varepsilon_y} \right)_j \cdot \left( \frac{\partial \varepsilon_y}{\partial u_y} \right)_j = \left( \frac{\partial \sigma_y}{\partial \varepsilon_y} \right)_j \cdot \frac{b_j \cdot t}{h} \quad (2.4)$$

$$k_{H,j} = \left( \frac{\partial F_H}{\partial u_H} \right)_j = \left( \frac{\partial F_H}{\partial \tau_{xy}} \right)_j \cdot \left( \frac{\partial \tau_{xy}}{\partial \gamma_{xy}} \right)_j \cdot \left( \frac{\partial \gamma_{xy}}{\partial u_H} \right)_j = \left( \frac{\partial \tau_{xy}}{\partial \gamma_{xy}} \right)_j \cdot \frac{b_j + h}{2} \cdot \frac{t}{h} \quad (2.5)$$

Resulting internal axial and shear forces in the panel elements are then determined as:

$$F_{x,j} = \sigma_{x,j} \cdot h \cdot t \quad (2.6)$$

$$F_{y,j} = \sigma_{y,j} \cdot b_j \cdot t \quad (2.7)$$

$$F_{xy,j} = \tau_{xy,j} \cdot \frac{b_j + h}{2} \cdot t \quad (2.8)$$

In equations (2.3) to (2.8)  $h$  is the model element height,  $b_j$  is the width of  $j$ -th panel element and  $t$  is the wall thickness.

Since the displacements along the six nodal degrees of freedom  $\{\delta_N\}$  and deformations along the  $m$  extensional degrees of freedom  $\{\delta_x\}$  are assumed to be kinematically independent, the model element stiffness matrix is a combined matrix consisting of two sub-matrices  $[K_e]^N$  and  $[K_e]^x$ , given by the following expression:

$$[K_e] = \begin{bmatrix} [K_e]^N & [0] \\ [0] & [K_e]^x \end{bmatrix} \quad (2.9)$$

Sub-matrix  $[K_e]^N$  is the element stiffness matrix relative to the six nodal degrees of freedom  $\{\delta_N\}$  assembled from corresponding panel axial stiffness values in the vertical direction  $k_{y,j}$  and an element shear stiffness  $k_H$  ( $k_H = \Sigma k_{H,j}$ ), as described by Massone et al. (2006). Sub-matrix  $[K_e]^x$  is the element stiffness matrix corresponding to the  $m$  extensional degrees of freedom  $\{\delta_x\}$ , and is expressed as a diagonal matrix:

$$[K_e]^x = \text{diag}\{k_{x,1} \quad k_{x,2} \quad \dots \quad k_{x,m}\}; \quad (2.10)$$

Similarly, the corresponding internal force vector of the model element can be written as:

$$\{F_{e,int}\} = \begin{Bmatrix} \{F_{e,int}\}^N \\ \{F_{e,int}\}^x \end{Bmatrix} \quad (2.11)$$

where  $\{F_{e,int}\}^N$  is the element force vector relative to the six nodal displacement degrees of freedom, and  $\{F_{e,int}\}^x$  is the element force vector corresponding to the  $m$  extensional degrees of freedom. The element force sub-vector  $\{F_{e,int}\}^N$  is derived from the resulting axial ( $F_{y,j}$ ) and shear ( $F_{xy,j}$ ) forces in panel elements as described by Orakcal et al. (2004), while the element force sub-vector  $\{F_{e,int}\}^x$  relative to the extensional degrees of freedom is given by:

$$\{F_{e,int}\}^x = \{F_{x,1} \quad F_{x,2} \quad \dots \quad F_{x,m}\}^T; \quad (2.12)$$

A displacement-controlled iterative solution strategy, based on a specified increment of a selected displacement component, was adopted in this study for conducting the nonlinear analyses. Iterations are performed on both displacement and load components to obtain equilibrium within a specified tolerance, while keeping the value of the selected displacement component (e.g., wall top displacement) constant.

In the model formulation presented here the resultant transverse normal stress  $\sigma_x$  within each panel macro-fiber (resultant of the contributions from concrete and reinforcing steel), was assumed to be zero, which is consistent with the boundary conditions with no transverse loads applied over the wall height (except at the top). Previous studies performed by Massone et al. (2006) revealed that the zero resultant horizontal stress assumption is not capable of correctly reproducing experimental responses observed in walls with low shear span-to-depth ratios (lower than approximately 0.5), underestimating the lateral load capacity of the wall by 13% to 40%. This study, however, focuses on the application of the proposed modeling approach, with the implemented assumption of zero resultant horizontal stress along the length of the wall ( $\sigma_x = 0$ ), to cantilever walls with aspect ratios larger than 1.0.

### 3. TEST PROGRAM

Experimental data used to validate the proposed analytical model was obtained from a recent test program designed particularly to investigate factors that influence the deformation capacity of moderate aspect ratio walls. The test program included five large-scale RC wall specimens, either 183 cm (72 in) or 244 cm (96 in) tall, 122 cm (48 in) long, and 15.2 cm (6 in) thick; therefore resulting shear-span-to-depth ratios are 1.5 and 2.0, respectively. The design compressive strength of concrete was 34.5 MPa (5,000 psi), whereas the reinforcing steel bars were primarily Grade 60 ( $f_y = 420$  MPa). Basic information on the test specimens, including dimensions, applied levels of axial load, web reinforcement ratios in horizontal and vertical directions ( $\rho_t$  and  $\rho_l$ ), boundary reinforcement ratios ( $\rho_b$ ), and nominal shear strengths ( $V_n$ ) are presented in Table 3.1. A detailed description of the experimental program and the test results can be found in the paper by Tran and Wallace (2012).

All test specimens were equipped with an extensive set of instrumentation to enable the collection of detailed experimental data at both global and local (deformation) response levels. Strains on the reinforcement were measured using approximately 30 strain gauges on each specimen at different locations, while 45 LVDTs (Linear-Variable-Differential-Transducers) were used to measure average concrete strains. The LVDTs were configured to measure the distribution of the average vertical, horizontal and shear strains at multiple locations over the wall height to enable the determination of

the contributions of shear and flexural deformations to wall lateral displacements, as well as to monitor the sliding and the rotation of the pedestal. The detailed experimental data obtained from this test program is used to assess the ability of the proposed modeling approach to capture the measured global and local responses and to identify areas of potential model improvements.

**Table 3.1.** Test matrix

| Spec. <sup>(1)</sup><br>No. | Spec.<br>name       | $h_w/l_w$ | $h_w$<br>(cm) | $l_w$<br>(cm) | $t_w$<br>(cm) | Axial<br>load ratio<br>$P/(A_g f'_c)$ | Web<br>reinforcement<br>ratio<br>( $\rho_t = \rho_l$ ) | Boundary<br>reinforcement<br>ratio<br>( $\rho_b$ ) | $V_n$<br>(kN) |
|-----------------------------|---------------------|-----------|---------------|---------------|---------------|---------------------------------------|--|--|---------------|
| SP 1                        | RW-A20-<br>P10-S38  | 2.0       | 244           | 122           | 15.2          | 0.10                                  | 0.27%  | 3.23%  | 427           |
| SP 2                        | RW-A20-<br>P10-S63  | 2.0       | 244           | 122           | 15.2          | 0.10                                  | 0.61%  | 7.11%  | 649           |
| SP 3                        | RW-A15-<br>P10-S51  | 1.5       | 183           | 122           | 15.2          | 0.10                                  | 0.32%  | 3.23%  | 574           |
| SP 4                        | RW-A15-<br>P10-S78  | 1.5       | 183           | 122           | 15.2          | 0.10                                  | 0.73%  | 6.06%  | 836           |
| SP 5                        | RW-A15-<br>P2.5-S64 | 1.5       | 183           | 122           | 15.2          | 0.05                                  | 0.61%  | 6.06%  | 743           |

<sup>(1)</sup> used in further text when referring to test specimens for convenience

#### 4. ANALYTICAL MODELING STUDIES

Experimental data obtained for two RC wall specimens, SP 2 ( $h_w/l_w = 2.0$ ) and SP 4 ( $h_w/l_w = 1.5$ ), are used to investigate the robustness of the proposed modeling approach. Both test walls are designed to yield in flexure prior reaching the nominal shear capacity, but with relatively higher shear stress; therefore SFI is expected (i.e., both nonlinear flexure and shear deformations are expected to significantly contribute to wall top lateral displacement). A limited set of preliminary results are presented here; a more detailed studies are underway.

Both specimens demonstrated nonlinear flexural and nonlinear shear behavior, with shear deformations contributing as much as 30% and 35% to the overall lateral displacements measured at the top of specimens SP 2 and SP 4, respectively. Concrete crushing at the wall boundaries, followed by the buckling of longitudinal boundary reinforcement caused lateral strength degradation for both specimens, ultimately resulting in large sliding shear deformations observed at the base of the walls, under the displacement-controlled, reversed-cyclic lateral loading.

A cyclic top displacement history, consistent with that applied to the test walls, was applied to the model; however, for this preliminary study only one loading cycle was applied at each drift level versus two or three in the actual test. A constant axial load corresponding to the resultant of the forces applied by the vertical actuators (approximately 640 kN (144 kips)) was applied at the top of each wall model. The constitutive material models were calibrated to match the as-tested material properties for both concrete and reinforcing steel by using results of uniaxial loading tests conducted on concrete cylinders and reinforcing steel coupon samples. Specimens SP 2 and SP 4 were modeled using 6 and 5 elements stacked along the height of the wall, respectively, while each model element consisted of 5 panel elements (panel-macro fibers) along the wall length. The effect of confinement on the stress-strain behavior of concrete was considered for the outermost panel elements, which represent the boundary elements of the walls. For each panel element, reinforcing steel was distributed uniformly, with different reinforcing ratios in the vertical and horizontal directions, according to the reinforcement details within the boundary regions and the web of the wall specimens.

##### 4.1. Lateral load vs. top displacement response

Comparisons of analytically-predicted and experimentally-measured lateral load versus top displacement for SP 2 and SP 4 are presented in Fig. 4.1. Overall, the comparisons indicate that the

analytical model captures reasonably well the experimentally-measured lateral load versus displacement responses obtained for both specimens. The lateral load at yield for the walls is accurately predicted, and the lateral load predicted by the model is in good agreement with the test results for most of the drift levels. The modest drop in lateral load in the analysis results, at a drift level of roughly 2.0%, is related to crushing of concrete in the panel elements at the wall boundaries; use of a more refined model discretization within the wall boundary regions (e.g., two panels for each boundary region instead of one) might improve the model results. The lateral stiffness of the walls is predicted reasonably well by the model, except for the initial loading cycles prior to yielding (up to the drift level of 0.5%) where the model stiffness is slightly higher than that for the test walls.

Cyclic properties of the response, including degradation in the unloading/reloading stiffness as well as the residual (plastic) displacements, are accurately represented by the model results. However, the overall shape of the hysteretic loops predicted by the model deviates from the experimental results; the model does not capture the pinching behavior observed in the tests. To investigate possible reasons for this discrepancy, the flexural and shear deformation components of the walls were examined.

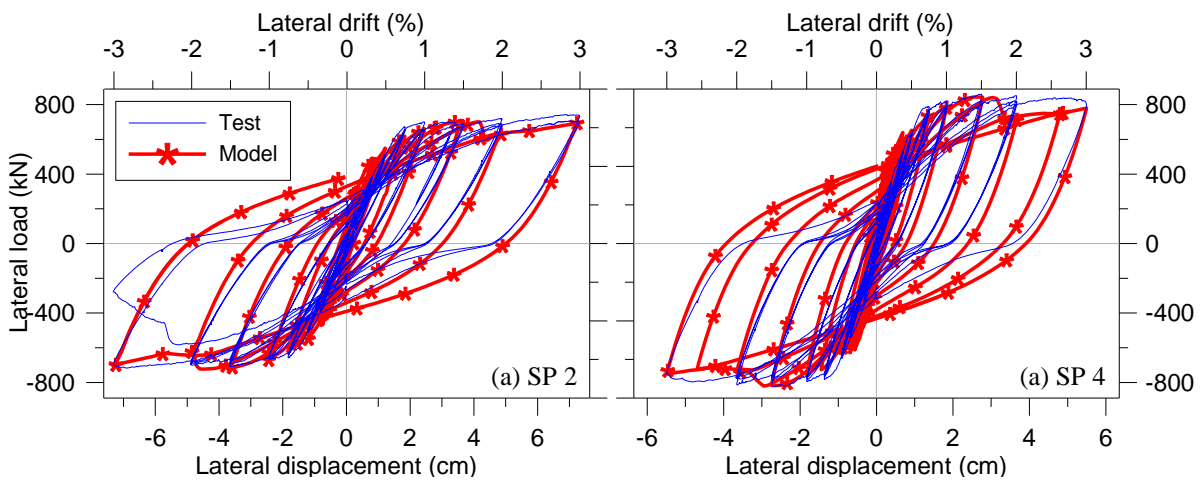


**Figure 4.1.** Lateral load vs. wall top displacement: (a) specimen SP 2, and (b) specimen SP 4

#### 4.2. Flexural and shear deformation components

The relative contributions of flexure and shear deformations to the top lateral displacement response of the walls are plotted in Fig. 4.2 and Fig. 4.3 for specimens SP 2 and SP 4, respectively. Local flexural and shear deformation measurements obtained from vertical and diagonal LVDTs were used to determine the experimental relations, whereas shear deformation in the analytical model is related to the shear strain on the panel macro-fibers in each model element. Comparisons of the analytical and experimental results indicate that analytical model is able to capture the presence of wall nonlinear shear deformations, which are coupled with nonlinear flexural deformations, through the entire cyclic loading history. However, the relative magnitudes of the contributions are not accurately predicted (Fig. 4.4), as the analytical model overestimates flexural deformations by approximately 30%, and underestimates the shear deformations by approximately 30% to 40% at all drift levels. As well, the model was unable to capture the sliding shear deformations observed along the base of both wall specimens near the end of the tests. These sliding deformations did not occur at the wall-foundation interface, but occurred over the highly damaged region just above the foundation-wall interface. Furthermore, although the overall hysteretic shape of the lateral load versus flexural displacement response is predicted reasonably well, the pronounced pinching behavior observed in the lateral load versus shear responses (Fig. 4.2b and Fig. 4.3b) of the test walls were not captured by the model.

Sensitivity studies conducted by varying model parameters revealed that discrepancies between the model results and test measurements are mainly due to the simple linear-elastic constitutive relationship adopted in the model formulation (Eq. 2.1), to relate sliding shear strain with the shear

stress along crack surfaces. The results presented are for linear-elastic, near rigid aggregate interlock behavior, which underestimated shear deformations and overestimated flexural deformations, and did not account for the “pinched” load versus shear deformation response reflected in the shape of the overall load versus displacement response. An alternative formulation with zero aggregate interlock stresses along the cracks (not shown here for brevity) predicts much larger shear deformations, as well as highly-pinched load versus shear deformation responses, but also resulted in significant underestimation of the wall lateral load capacity.

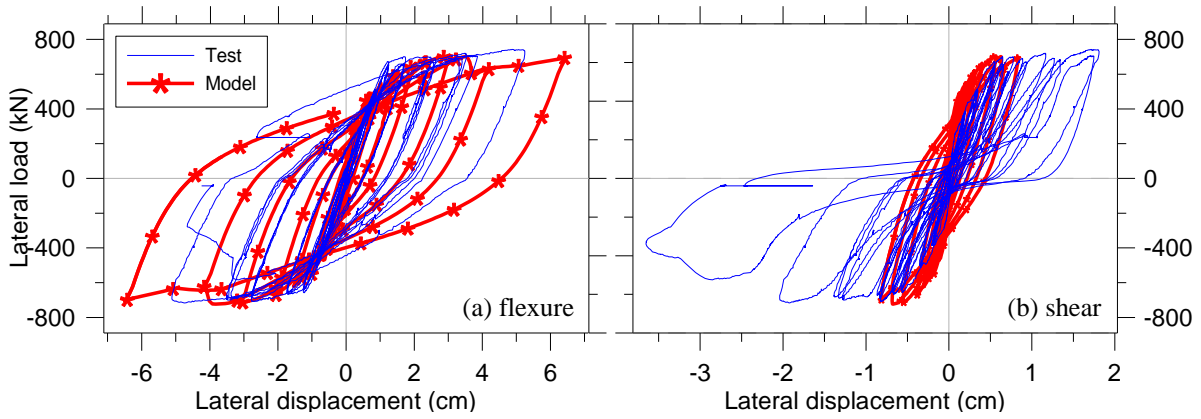


**Figure 4.2.** Lateral load vs. top displacement components for specimen SP 2: (a) flexure, (b) shear

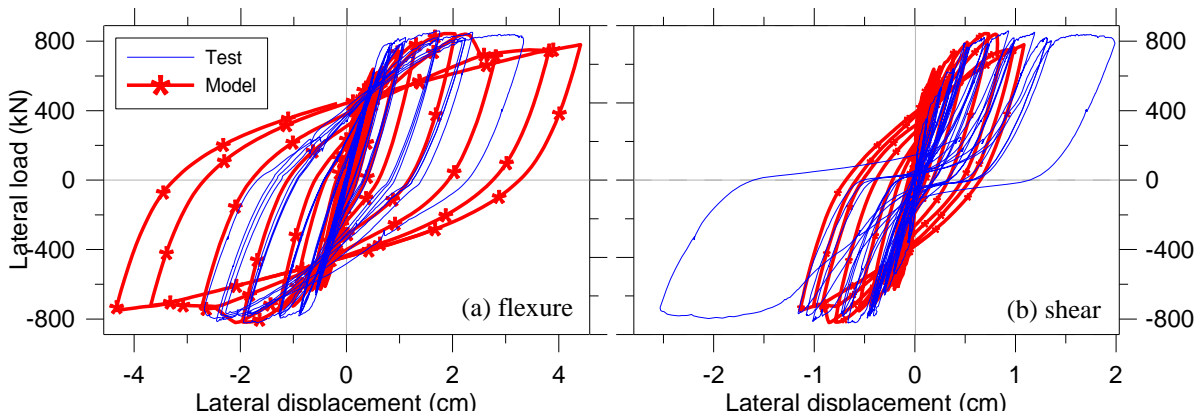


**Figure 4.3.** Lateral load vs. top displacement components for specimen SP 4: (a) flexure, (b) shear

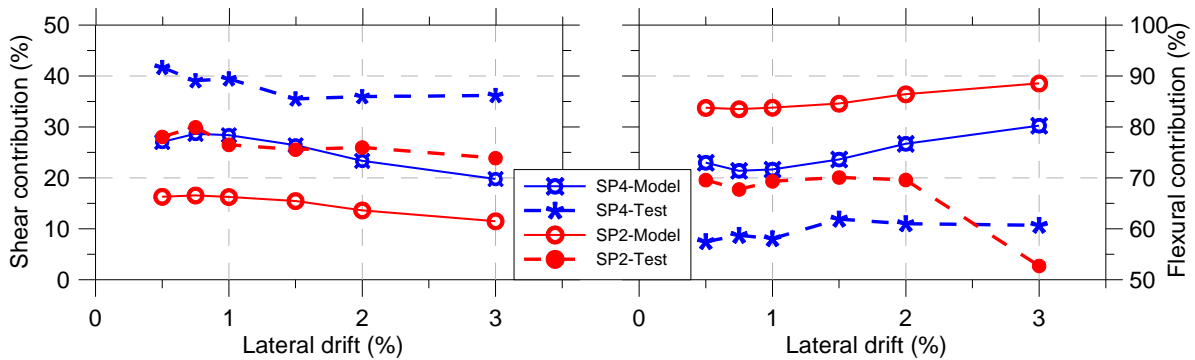


**Figure 4.4.** Shear and flexural components of top displacement for specimens SP 2 and SP 4: (a) shear, (b) flexure

Use of a linear-elastic (somewhat rigid) aggregate interlock assumption produces reasonably good comparisons between model and test results for conditions where a diagonal crack is closed and the compressive stresses are acting perpendicular to the crack; however, when the crack is opened, the

rigid interlock assumption becomes unrealistic and results in significant overestimation of the shear stiffness of a panel element, especially during load reversal stages where pronounced pinching is observed. Current research is focused on developing a more refined constitutive relationship for aggregate interlock behavior to improve response predictions. However, even with the linear elastic aggregate interlock assumption, the model results reasonably capture wall responses, including the lateral load capacity and deformation components, primarily because significant sliding along diagonal cracks was not observed during the tests.

### 4.3. Crack patterns

The crack directions predicted by the analytical model in each of the panel elements are compared with cracks observed in the two wall tests in Fig. 4.5.

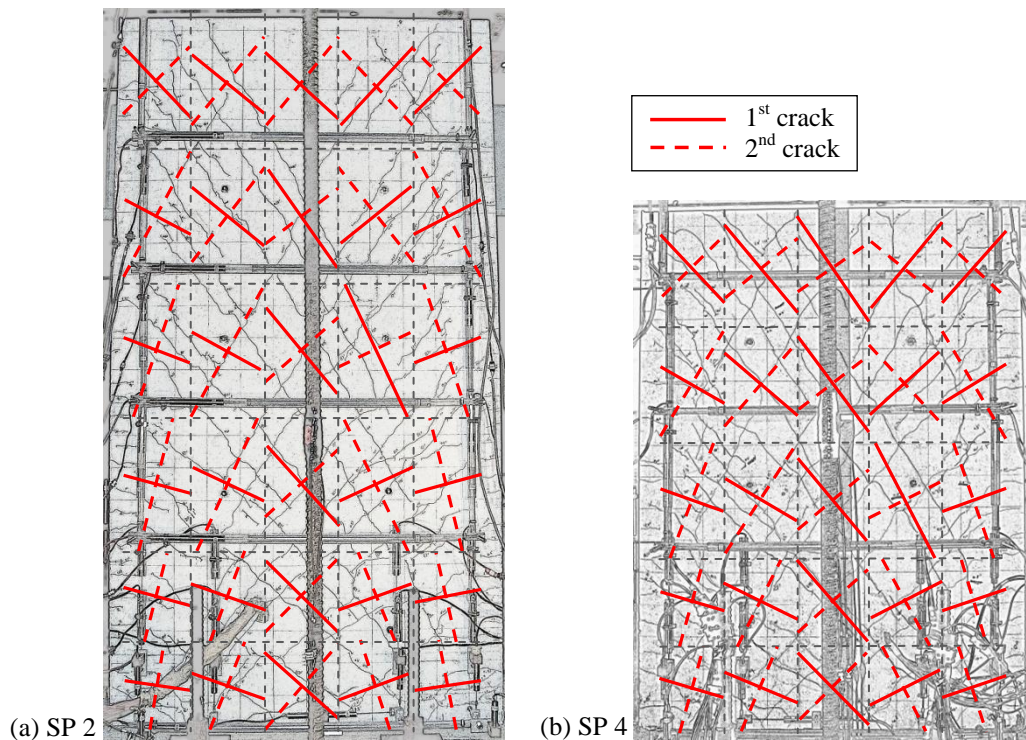


**Figure 4.5.** Comparison of crack patterns and model discretization: (a) specimen SP 2, (b) specimen SP 4

Overall, the orientation of cracks predicted by the model reasonably agree with the crack orientations observed on the test specimens, verifying that the model captures the principal tensile strain directions in the wall tests. This result suggests that the assumption of zero resultant horizontal stress ( $\sigma_x = 0$ ) on each panel element used along the length of the wall is appropriate for walls with moderate aspect ratio. The model also incorporates the assumption that the second crack that forms in each panel element is perpendicular to orientation of the first crack, which is not strictly observed in the tests. Potential revisions to the assumption of the orthogonal-crack formulation used in the model may improve crack pattern predictions.

## 5. SUMMARY AND CONCLUSIONS

An analytical model, which considers the interaction between flexural and shear behavior, is proposed for predicting of the nonlinear response of moderate-aspect ratio reinforced concrete walls under reversed cyclic loading. The model formulation incorporates RC panel behavior, described by a fixed-strut-angle approach, into the fiber-based Multiple Vertical Line Element Model (MVLEM). To verify the modeling approach and assumptions, analytical model predictions were compared with

experimental data obtained in recent tests of two walls (aspect ratios of 1.5 and 2.0) in which significant shear-flexure interaction responses were measured. In general, model results reasonably represented the test results in terms of load versus top lateral displacement, indicating the promise of proposed modeling approach and also helping to identify ways to improve the model formulation.

The model overestimates flexural deformations by approximately 30%, underestimates shear deformations by 30% to 40%, and does not capture the pinching behavior observed in the experimental load versus overall displacement and load versus shear deformation responses. These discrepancies are attributed to the fairly simple linear-elastic shear aggregate interlock relation used in the preliminary model formulation.

Ongoing studies are focusing on refinement of the model assumptions to improve model response predictions as well as further experimental validation of the model for a wider range of RC wall configuration (e.g. geometric properties, reinforcing details, material strengths).

## REFERENCES

- Barda, F., Hanson, J. M., and Corley, W. G. (1976). Shear strength of low-rise walls with boundary elements. *Research and development Bulletin*, construction technology laboratories, Portland Cement Association, **RD043.01D**, 19
- Beyer K., Dazio A., M. J. Nigel Priestley (2011). Shear Deformations of Slender Reinforced Concrete Walls under Seismic Loading. *ACI Structural Journal* **108:S17**, 167 - 177.
- Chang, G.A. and Mander J.B. (1994). Seismic Energy Based Fatigue Damage Analysis of Bridge Columns: Part I-Evaluation of Seismic Capacity. *NCEER Report No. 94-0006*, National Center for Earthquake Engineering Research.
- Filippou, F.C., E.G. Popov and V.V. Bertero (1994). Effects of Bond Deterioration on Hysteretic Behavior of Reinforced Concrete Joints. *EERC Report No. UCB/EERC-83/19*. University of California, Berkeley, 1983.
- Massone, L. M., Orakcal, K., and Wallace, J. W. (2006). Shear - Flexure Interaction for Structural Walls. *ACI Special Publication – Deformation Capacity and Shear Strength of Reinforced Concrete Members Under Cyclic Loading* **SP-236**, 127-150.
- Massone, L. M., and Wallace, J. W. (2004). Load-deformation responses of slender reinforced concrete walls. *ACI Structural Journal* **101:1**, 103-113.
- Menegotto, M. and Pinto E. (1973) Method of Analysis for Cyclically Loaded Reinforced Concrete Plane Frames Including Changes in Geometry and Non-Elastic Behavior of Elements under Combined Normal Force and Bending. *Proceedings, IABSE Symposium on Resistance and Ultimate Deformability of Structures Acted on by Well-Defined Repeated Loads*, Lisbon, Portugal, 1973.
- Orakcal, K., Wallace, J. W., and Conte, J. P. (2004). Nonlinear Modeling and Analysis of Slender Reinforced Concrete Walls. *ACI Structural Journal* **101:5**, 688 - 699.
- Orakcal, K., Wallace, J.W. (2006). Flexural Modeling of Reinforced Concrete Walls-Experimental Verification. *American Concrete Institute Structural Journal*. **103:2**, 196-206.
- Pang, D. and T.C. Hsu. Fixed Angle Softened Truss Model for Reinforced Concrete. *ACI Structural Journal* **93:2**, 197-207.
- S.Y. Xu and J. Zhang (2010). Hysteretic shear-flexure interaction model of reinforced concrete columns for seismic response assessment of bridges. *Earthquake Engineering and Structural Dynamics* **10.1002/eqe.1030**.
- Tran, T., Wallace, J., (2012). Experimental Study of Nonlinear Flexural and Shear Deformations of Reinforced Concrete Structural Walls. *15th World Conference on Earthquake Engineering*, Lisbon, Portugal.
- Ulugtekin, D. (2010). Analytical Modeling of Reinforced Concrete Panel Elements Under Reversed Cyclic Loadings. *M.S. Thesis*, Department of Civil Engineering, Bogazici University.